390968 - 2 - T

Diffraction By Parallel Resistive Half Plane Structures

John R. Natzke and John L. Volakis

Northrop Corporation
B2 Division
8900 E. Washington Blvd.
Pico Rivera CA

November 1992

390968-2-T = RL-2580

Diffraction By Parallel Resistive Half Plane Structures

John R. Natzke and John L. Volakis

Abstract

In Part I of this report, the diffraction of a resistive half plane over a planar resistive sheet under plane wave illumination is determined via the dual integral equation method (a variation of the Wiener-Hopf method). The solution is obtained upon splitting the associated Wiener-Hopf functions via a numerically efficient routine. Based on the derived exact half plane diffraction coefficient, a simplified equivalent model of the structure is developed when the separation of the half plane and resistive plane is on the order of a tenth of a wavelength or less. The model preserves the geometrical optics field of the original structure for all angles and is based on an approximate image theory of the resistive plane. Good agreement is obtained with the diffracted field exact solution.

In Part II, a higher order diffraction model of two overlapping resistive half planes is developed. The model is based on viewing the overlapping section between the edges of the half planes as a two port resistive parallel plate waveguide. The coupling, reflection, and launching coefficients of the waveguide modal fields are derived for each port via the dual integral equation method, and the multiple interactions are accounted for using a transmission line analysis. The results are verified by comparison with a method of moments solution. A simplified equivalent model of the structure is developed when the separation of the half planes is on the order of a hundreth of a wavelength or less. The geometrical optics field of the original structure is preserved for all angles, and the diffracted field of the simplified model is in good agreement with the higher order diffraction solution for the resistivities of concern.

Part I
Characterization of a Resistive Half Plane Over a Resistive Sheet

The angular spectrum method set forth by Booker and Clemmow [1] has been applied to many diffracting structures composed of a half plane over a substrate [2], [3], [4], [5], [6]. In many cases resistive sheets [7] are used over dielectric layers for radar cross section control, transmittivity control, or other applications. Also, when the dielectric layer is thin, it can be equivalently replaced by a resistive sheet.

In this report we particularly consider the diffraction by a resistive half plane vertically displaced from a uniform resistive sheet (see Fig. 1). The corresponding exact diffraction coefficient is derived for this configuration with an H-polarized illumination using the dual integral equation method, following a development similar to that in [5], [8]. The encountered Wiener-Hopf split function is factorized via an efficient numerical procedure discussed in [9].

When the separation between the resistive half plane and resistive sheet is on the order of a tenth of a wavelength or less, the structure is virtually planar. Thus a simplified model of the original configuration is a single equivalent resistive half plane illuminated by a direct and an image wave. This model relies on image theory to remove the lower planar sheet by introducing an image field and a second half plane placed symmetrically below the original resistive sheet. The two half planes are then combined into a single one with an equivalent resistivity such that the geometrical optics field of the original structure is preserved everywhere. The diffraction coefficient for this equivalent half plane is much simpler and given by [10]. Several patterns are presented for assessing the model's accuracy for various resistivities and separation distances. This is done by comparison with the exact solution which is in turn validated using a moment method solution.

1 Dual-integral equation formulation

Consider a resistive half plane of resistivity R_1, placed a distance d above a planar resistive sheet of resistivity R as shown in Fig. 1. Mathematically, the resistive half plane and the uniform resistive sheet satisfy the boundary conditions

$$\hat{y} \times \hat{y} \times \bar{E} = -R_1 \hat{y} \times [\bar{H}^+ - \bar{H}^-] \qquad y = 0, \quad x > 0 \tag{1}$$

$$\hat{y} \times \hat{y} \times \bar{E} = -R \hat{y} \times [\bar{H}^+ - \bar{H}^-] \qquad y = -d, \quad -\infty < x < \infty \tag{2}$$

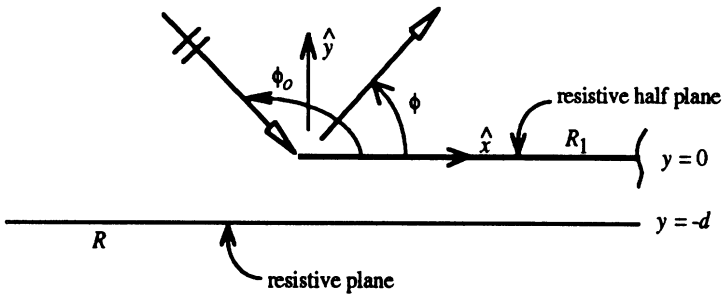

Figure 1: Geometry of the resistive half plane over an infinite resistive sheet.

in which $\bar{H}^{\pm}$ denotes the total magnetic field above and below the appropriate resistive sheet and $\bar{E}$ is likewise the total electric field which is continuous across the sheets.

Assume the plane wave

$$\bar{H}^i = \hat{z} e^{jk\rho\cos(\phi-\phi_0)} \tag{3}$$

is impinging upon the structure in Fig. 1, where k is the wavenumber, (ρ, ϕ) is the usual cylindrical coordinates and ϕ_0 is the angle of incidence such that $0 < \phi_0 < \pi$. For this excitation the total field may be represented as

$$H_z = H_z^i + H_z^r + H_z^s \tag{4}$$

in the region $y > -d$ and as

$$H_z = H_z^t + H_z^s \tag{5}$$

when $y < -d$. We identify H_z^r and H_z^t as the reflected and transmitted fields, respectively, of the planar resistive sheet satisfying (2). Namely

$$H_z^r = -\Gamma(\sin\phi_0)\, e^{-j2kd\sin\phi_0} e^{jk\rho\cos(\phi+\phi_0)} \tag{6}$$

$$H_z^t = T(\sin\phi_0)\, e^{jk\rho\cos(\phi-\phi_0)}, \tag{7}$$

where

$$\Gamma(\sin\phi_0) = -\frac{\sin\phi_0}{\eta + \sin\phi_0} \tag{8}$$

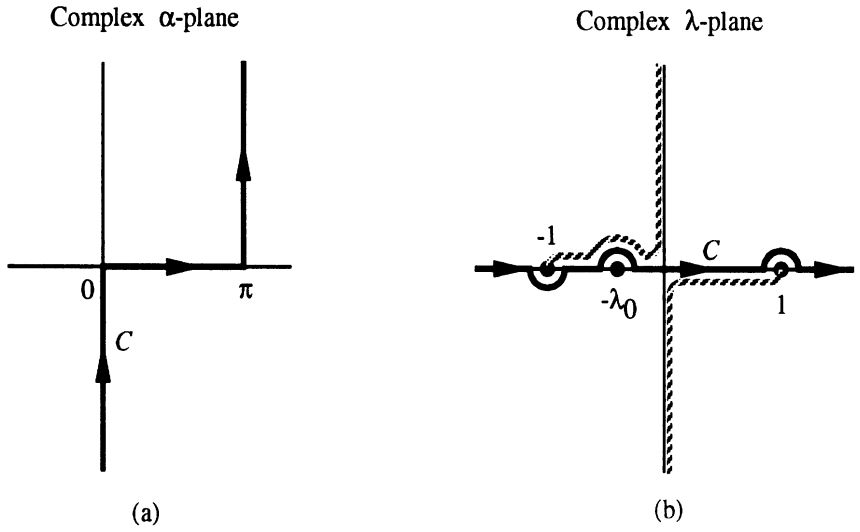

Figure 2: Illustration of the C contour in the α- and λ-planes.

and

$$T(\sin\phi_0) = 1 + \Gamma(\sin\phi_0) \tag{9}$$

are the plane wave reflection and transmission coefficients in which $\eta = 2R/Z_0$. Further, we identify H_z^s in (4) and (5) as the scattered field caused by the presence of the half plane at $y = 0$. In the absence of the uniform infinite resistive sheet, this field is due to currents excited on the isolated half plane which can be represented by the angular spectral integral [11]

$$H_z^{s1} = \pm \int_C P(\cos\alpha)\, e^{-jk\rho\cos(\phi\mp\alpha)}\, d\alpha, \quad y \gtrless 0 \tag{10}$$

where the contour C is defined in Fig. 2 and $P(\cos\alpha)$ is the unknown spectra proportional to the current on the half plane. In the presence of the resistive plane at $y = -d$, this field generates additional reflections from (and transmissions through) the plane. Treating (10) as a sum of plane waves, the total scattered field becomes

$$H_z^s = \int_C \left[1 + \Gamma(\sin\alpha)\, e^{-j2kd\sin\alpha}\right] P(\cos\alpha)\, e^{-jk\rho\cos(\phi-\alpha)}\, d\alpha \tag{11}$$

for $y > 0$,

$$H_z^s = -\int_C \left[e^{-jk\rho\cos(\phi+\alpha)} - \Gamma(\sin\alpha)\, e^{-j2kd\sin\alpha} e^{-jk\rho\cos(\phi-\alpha)}\right] P(\cos\alpha)\, d\alpha \tag{12}$$

for $-d < y < 0$, and

$$H_z^s = -\int_C T(\sin\alpha)\, P(\cos\alpha)\, e^{-jk\rho\cos(\phi+\alpha)}\, d\alpha \tag{13}$$

for $y < -d$.

In the following we shall invoke the appropriate boundary conditions to determine the unknown spectra $P(\cos\alpha)$. First, to maintain the continuity of the total magnetic field across $x < 0$, $y = 0$, the condition $\hat{y}\times(\bar{H}^+ - \bar{H}^-) = 0$ must be satisfied. Upon using (3), (6), (11) and (12) in conjunction with (4), this condition implies

$$H_z^{s+} - H_z^{s-} = 2\int_C P(\cos\alpha)\, e^{-jkx\cos\alpha}\, d\alpha = 0, \quad x < 0.$$

On setting $\lambda = \cos\alpha$, this can be rewritten as

$$\int_{-\infty}^{\infty} \frac{P(\lambda)}{\sqrt{1-\lambda^2}}\, e^{-jkx\lambda}\, d\lambda = 0, \quad x < 0, \tag{14}$$

and the path of integration is shown in Fig. 2. Since this integral equation is valid only for $x < 0$, the path of integration can be closed by a semi-infinite circle in the upper λ-plane without altering the result of the integration. From Cauchy's theorem, $P(\lambda)/\sqrt{1-\lambda^2}$ must then be free of zeros, branch cuts, or any other singularities in the upper half plane. Consequently, we can state that

$$\frac{P(\lambda)}{\sqrt{1-\lambda^2}} = U(\lambda) \tag{15}$$

where $U(\lambda)$ is a function regular in the upper half of the λ-plane.

The application of (1) across the half plane $x > 0$, $y = 0$, leads to the integral equation

$$\begin{aligned} &\int_{-\infty}^{\infty} \left[\frac{\eta_1}{\sqrt{1-\lambda^2}} + 1 + \Gamma(\sqrt{1-\lambda^2})\, e^{-j2kd\sqrt{1-\lambda^2}}\right] P(\lambda)\, e^{-jkx\lambda}\, d\lambda \\ = \;& \sqrt{1-\lambda_0^2}\left[1 + \Gamma\left(\sqrt{1-\lambda_0^2}\right)\, e^{-j2kd\sqrt{1-\lambda_0^2}}\right] e^{jkx\lambda_0}, \quad x > 0, \end{aligned} \tag{16}$$

in which $\eta_1 = 2R_1/Z_0$ and $\lambda_0 = \cos\phi_0$. Since (16) is valid only for $x > 0$, the path of integration may now be closed by a semi-infinite circle in the lower half of the λ-plane. On applying Cauchy's theorem we then obtain the functional equation

$$Q(\lambda)\frac{P(\lambda)}{\sqrt{1-\lambda^2}} = -\frac{1}{2\pi j}\frac{L(\lambda)}{L(-\lambda_0)}\frac{\sqrt{1-\lambda_0^2}}{\lambda+\lambda_0}\, A\left(\sqrt{1-\lambda_0^2}\right) \tag{17}$$

where

$$Q(\lambda) = \eta_1 + \sqrt{1-\lambda^2}\left[1 + \Gamma(\sqrt{1-\lambda^2})\, e^{-j2kd\sqrt{1-\lambda^2}}\right] \quad (18)$$

$$A\left(\sqrt{1-\lambda_0^2}\right) = 1 + \Gamma\left(\sqrt{1-\lambda_0^2}\right) e^{-j2kd\sqrt{1-\lambda_0^2}} \quad (19)$$

and $L(\lambda)$ is a function regular in the lower half of the λ-plane.

To proceed further, $Q(\lambda)$ must first be factorized as a product of upper and lower half plane functions. In light of (8), we write (18) as

$$Q(\lambda) = \frac{U_w(\lambda)\, L_w(\lambda)}{U_s(\lambda)\, L_s(\lambda)} \quad (20)$$

where

$$U_w(\lambda)\, L_w(\lambda) = (\eta_1 + \sqrt{1-\lambda^2})(\eta + \sqrt{1-\lambda^2}) - (1-\lambda^2)e^{-j2kd\sqrt{1-\lambda^2}} \quad (21)$$

and

$$U_s(\lambda)\, L_s(\lambda) = \eta + \sqrt{1-\lambda^2}. \quad (22)$$

Here $U_w(\lambda)$ and $U_s(\lambda)$ denote upper half plane functions and $L_w(\lambda)$ and $L_s(\lambda)$ denote lower half plane functions. The factorization of (21) can be accomplished using numerical methods [3]. For the case of (22), the known factorization [12]

$$\left(\gamma + \frac{1}{\sqrt{1-\lambda^2}}\right)^{-1} = K_+(\lambda,\gamma)\, K_-(\lambda,\gamma) \quad (23)$$

is noted, resulting in

$$U_s(\lambda) = \sqrt{\eta}\, \frac{\sqrt{1-\lambda}}{K_+(\lambda, 1/\eta)} = L_s(-\lambda). \quad (24)$$

Explicit, non-integral expressions for $K_+(\lambda,\gamma)$ are given in [13] for $\mathrm{Re}(\gamma) > 0$. If $\mathrm{Re}(\gamma) < 0$, then $K_+(\lambda,\gamma)$ must be replaced with the expression [4]

$$j\frac{1}{\gamma}\, \frac{\lambda - \sqrt{1-\gamma^2}}{K_+(\lambda,-\gamma)}.$$

Returning now to (17), upon making use of (20) and (15), we obtain

$$\left\{\frac{U_w(\lambda)}{U_s(\lambda)}\, U(\lambda)\right\}\left\{\frac{L_w(\lambda)}{L_s(\lambda)}\right\} = -\frac{1}{2\pi j}\, \frac{L(\lambda)}{L(-\lambda_0)}\, \frac{\sqrt{1-\lambda_0^2}}{\lambda + \lambda_0}\, A\left(\sqrt{1-\lambda_0^2}\right).$$

To assure regularity of $U(\lambda)$ and $L(\lambda)$ in their respective planes, it is clear that

$$L(\lambda) = \frac{L_w(\lambda)}{L_s(\lambda)},$$

and from (17) we obtain that

$$P(\lambda) = -\frac{1}{2\pi j}\frac{\sqrt{1-\lambda^2}\sqrt{1-\lambda_0^2}}{\lambda+\lambda_0} A\left(\sqrt{1-\lambda_0^2}\right)\frac{U_s(\lambda)}{U_w(\lambda)}\frac{L_s(-\lambda_0)}{L_w(-\lambda_0)}. \tag{25}$$

This is proportional to the spectrum of the current on the resistive half plane in the presence of the resistive sheet at $y = -d$.

The far zone scattered field is determined by substituting the spectral function $P(\lambda)$ as given by (25) into (11) and (13) and evaluating the integrals via the steepest descent method. Doing so, we obtain the form

$$H_z^s \simeq \frac{e^{-jk\rho}}{\sqrt{\rho}} S^{(1)}(\phi, \phi_0) \tag{26}$$

where $S^{(1)}(\phi, \phi_0)$ is often denoted as the diffraction coefficient of the configuration and is given by

$$S^{(1)}(\phi, \phi_0) = -\frac{e^{-j\frac{\pi}{4}}}{\sqrt{2\pi k}} \left\{ \begin{matrix} A(\sin\phi) \\ T(-\sin\phi) \end{matrix} \right\} A(\sin\phi_0) \frac{\sin\phi \sin\phi_0}{\cos\phi + \cos\phi_0} \cdot \frac{U_s(\cos\phi)\, U_s(\cos\phi_0)}{U_w(\cos\phi)\, U_w(\cos\phi_0)} \tag{27}$$

for $\left\{ \begin{matrix} 0 < \phi < \pi \\ \pi < \phi < 2\pi \end{matrix} \right\}$. In deriving these expressions the identities $U_s(\lambda) = L_s(-\lambda)$ and $U_w(\lambda) = L_w(-\lambda)$ were employed. $S^{(1)}(\phi, \phi_0)$ is generally referred to as the diffraction coefficient of the upper resistive half plane in the presence of the lower sheet.

The diffracted field expressions can be verified for two limiting cases. When $\eta \to \infty$, the resistive sheet vanishes, and the diffraction coefficient becomes

$$\begin{aligned} S^{(1)}(\phi, \phi_0) &= D_H(\phi, \phi_0, \eta_1) \\ &= -\frac{2e^{-j\frac{\pi}{4}}}{\eta_1\sqrt{2\pi k}} \frac{\cos\frac{\phi}{2}\cos\frac{\phi_0}{2}}{\cos\phi + \cos\phi_0} K_+(\cos\phi, 1/\eta_1)\, K_+(\cos\phi_0, 1/\eta_1) \end{aligned} \tag{28}$$

as given in [9]. The other limiting case is $d \to 0$; in this case $S^{(1)}(\phi, \phi_0)$ reduces to

$$S^{(1)}(\phi, \phi_0) = \pm\frac{e^{-j\frac{\pi}{4}}}{\sqrt{2\pi k}}\left(\frac{1}{\eta} - \frac{1}{\eta_2}\right) \cdot \frac{K_+\left(-\cos\phi, \frac{1}{\eta}\right) K_+\left(-\cos\phi_0, \frac{1}{\eta}\right) K_+\left(\cos\phi, \frac{1}{\eta_2}\right) K_+\left(\cos\phi_0, \frac{1}{\eta_2}\right)}{\cos\phi + \cos\phi_0}, \quad y \gtrless 0. \tag{29}$$

This is recognized as the H-polarization diffraction coefficient of a junction formed by two coplanar resistive half planes as derived in [14]. The pertinent half planes have resistivities $R = 2Z_0/\eta$ $(x < 0)$ and $R_2 = 2Z_0/\eta_2$, $(x > 0)$, where $\eta_2 = \eta_1\eta/(\eta_1 + \eta)$.

2 Simplified model for small d

When the separation between the resistive half plane and lower resistive sheet is small (i.e. $kd \ll 1$), the structure is virtually planar, and it is possible and instructive to seek a simplification of the exact solution developed in the previous section. To do so we shall first construct an equivalent geometry which recovers the geometrical optics (GO) fields of the original one in Fig. 1. With this in mind, R can be removed by introducing an appropriate image of the resistive half plane and of the incident field as illustrated in Fig. 3. To recover the GO fields of the original geometry it is necessary to sum the GO fields associated with the pair of half planes in Fig. 3 under the direct (H_z^i) and imaged $(\widetilde{H}_z^r)$ illumination. In addition, an appropriate value for the resistivity $\tilde{R}_1$ of the imaged half plane must be specified. To determine $\tilde{R}_1$ and $\widetilde{H}_z^r$ we consider the GO fields of the original structure. The reflected field associated with its right side (side of the resistive half plane) is found to be

$$H_z^{r1} = -\left[\Gamma_1 + \frac{T_1^2\Gamma e^{-j2kd\sin\phi_0}}{1 - \Gamma_1\Gamma e^{-j2kd\sin\phi_0}}\right] e^{jk\rho\cos(\phi+\phi_0)}, \quad y > 0 \tag{30}$$

where Γ and T are defined in (8) and (9) and

$$\Gamma_1 = -\frac{\sin\phi_0}{\eta_1 + \sin\phi_0}, \qquad T_1 = \frac{\eta_1}{\eta_1 + \sin\phi_0} \tag{31}$$

with $\eta_1 = 2R_1/Z_0$. The appropriate reflected field for the left side of the same geometry can be obtained by letting $\eta_1 \to \infty$. The mechanisms leading to this expression are illustrated in Fig. 4 along with the equivalent ones associated with the new pair of sheets in Fig. 3 (dashed line should be compared with dashed and likewise solid lines should be compared with solid). On comparing the sum of the GO fields generated by the pair of sheets in Fig. 3 under the two illuminations with (30), we deduce that

$$\tilde{R}_1 = -\frac{Z_0}{2}\sin\phi_0\,\frac{1 + \Gamma_1\Gamma^2}{\Gamma_1\Gamma^2}$$

and

$$\widetilde{H}_z^r = \begin{cases} \tilde{\Gamma}H_z^r & \phi < \pi - \phi_0 \\ H_z^r & \phi > \pi - \phi_0 \end{cases}$$

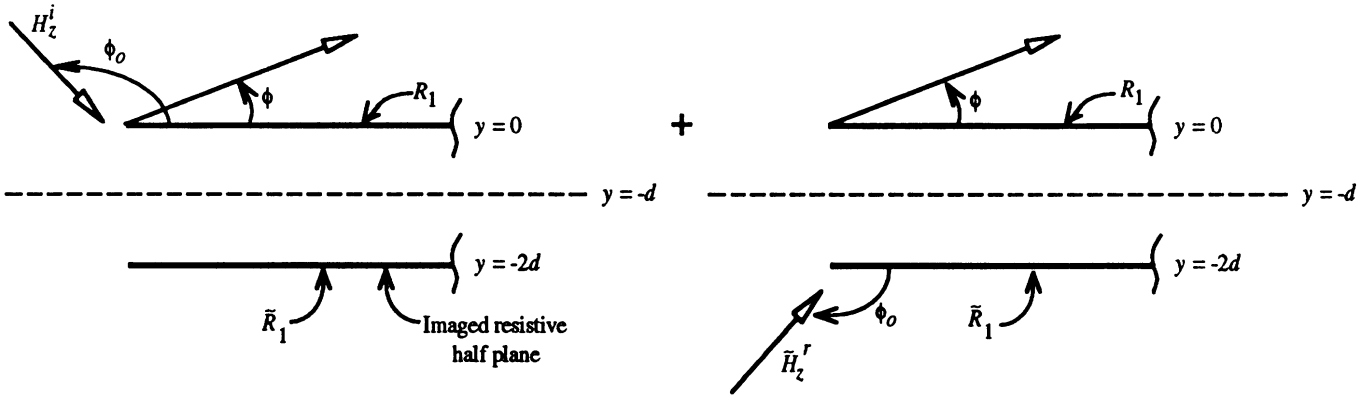

Figure 3: Intermediate equivalent geometry problem recovering the GO field ($y > 0$) of the structure in Fig. 1.

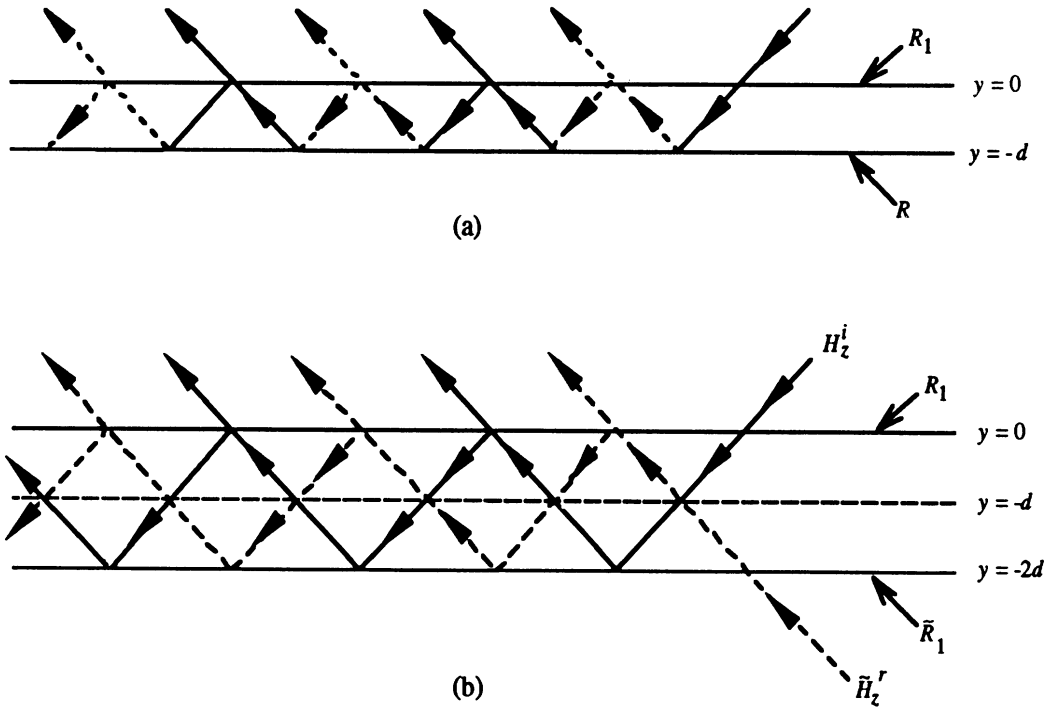

Figure 4: Illustration of the GO mechanisms associated with the original structure (Fig. 1) and the equivalent one in Fig. 3.

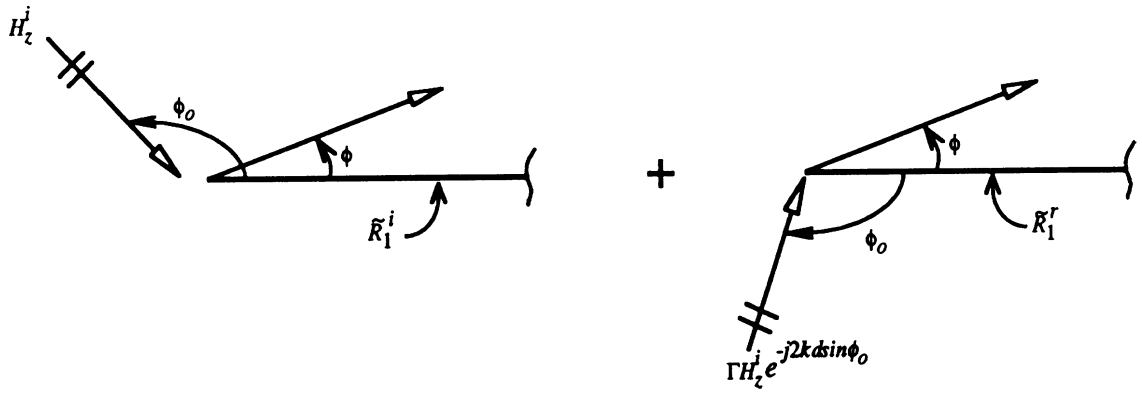

Figure 5: Equivalent set of single resistive half planes recovering the reflected GO field ($y > 0$) of the structure in Fig. 1. The half planes lie in the $y = -d$ plane.

in which

$$\tilde{\Gamma} = \frac{T_1}{1 + \Gamma_1 \Gamma^2}$$

and H_z^r is given in (6). Note that $\tilde{R}_1$ and $\tilde{\Gamma}$ are functions of the incidence angle since our requirement was to recover the GO fields of the original structure for all incidence angles.

Having determined the resistivity of the imaged half plane $\tilde{R}_1$, we now proceed to combine the pair of half planes into a single equivalent half plane at $x > 0$, $y = -q$, $0 < q < d$. This is illustrated in Fig. 5 and for each illumination a different resistivity is required. This can be determined by comparing the GO fields (reflected for the direct illumination and transmitted for the imaged illumination) of the configurations in Figs. 3 and 5 and requiring that they be equal. Doing so, we find that the resistivity of the single equivalent half plane subjected to direct illumination must be

$$\tilde{R}_1^i = -\frac{Z_0}{2} \sin\phi_0 \frac{1 + \tilde{\Gamma}_1^i}{\tilde{\Gamma}_1^i} \tag{32}$$

where

$$\tilde{\Gamma}_1^i = \Gamma_1 \left[1 + \frac{T_1^2 \Gamma^2 e^{-j4kd\sin\phi_0}}{1 - \Gamma_1^2 \Gamma^2 e^{-j4kd\sin\phi_0}} \right] e^{j2kq\sin\phi_0}. \tag{33}$$

When $q = 0$, the equivalent half plane is coincident with the original resistive half plane, and the equivalent resistivity $\tilde{R}_1^i$ was observed to have an average

value of R_1 as d was varied. When the dependence in ϕ_0 is also taken into account, an excellent approximation to $\tilde{R}_1^i$ is

$$\tilde{R}_1^i \simeq R_1 - (R_1 - \tilde{R}_2)e^{-j4kd\sin\phi_0}, \qquad q = 0 \tag{34}$$

where

$$\tilde{R}_2 = \frac{R_1\tilde{R}_1}{R_1 + \tilde{R}_1},$$

and this expression is the same as (32) and (33) with $d = 0$. We note that for $R_1 \lesssim R$, $(R_1 - \tilde{R}_2) \lesssim 0.2R_1$, and in that case we can approximate $\tilde{R}_i$ by R_1, its average value. For the cases when $q \neq 0$, the equivalent resistivity in (34) is transferred to a position $y = -q$ by preserving the GO fields of the original geometry. From (34) an approximate expression for $\tilde{R}_1^i$ is

$$\begin{aligned}\tilde{R}_1^i \simeq\ & \left[R_1 - (R_1 - \tilde{R}_2)e^{-j4kd\sin\phi_0}\right] e^{-j2kq\sin\phi_0} \\ & + \frac{Z_0}{2}\sin\phi_0\left(e^{-j2kq\sin\phi_0} - 1\right).\end{aligned} \tag{35}$$

We found that for far field scattering, the best results were obtained by setting $q = d$. That is, the accuracy of the model was not adequate when $\tilde{R}_1^i$ is replaced by its average value of R_1. It is necessary to retain the more accurate expressions for $\tilde{R}_1^i$ given by (32) or (35) which are, unfortunately, functions of the incidence angle.

For the imaged illumination, the corresponding half plane resistivity is found to be

$$\tilde{R}_1^r = \frac{Z_0}{2}\sin\phi_0\frac{\tilde{T}_1^r}{1 - \tilde{T}_1^r} \tag{36}$$

with

$$\tilde{T}_1^r = \frac{T_1^2}{1 - \Gamma_1^2\Gamma^2 e^{-j4kd\sin\phi_0}} \tag{37}$$

and the associated imaged field being set to H_z^r, $0 < \phi < \pi$. With this imaged field, the reflected field of Fig. 5(a) plus the transmitted field of Fig. 5(b) completely recover the GO field of the original configuration in the entire $y > 0$ region. Equations (36) and (37) show that $\tilde{R}_1^r \leq R_1/2$ as d and ϕ_0 are varied, although its average value is not a constant. We found, however, that if $R_1 \lesssim R$, the variation of $\tilde{R}_1^r$ with d and ϕ_0 is sufficiently small such that a good approximation is the constant

$$\tilde{R}_1^r \simeq \frac{Z_0}{2}\frac{\eta_1^2(\eta+1)^2}{(2\eta_1+1)(\eta+1)^2 - 1} \tag{38}$$

which is the expression reduced from (36) and (37) on setting $d = 0$ and $\phi_0 = \pi/2$.

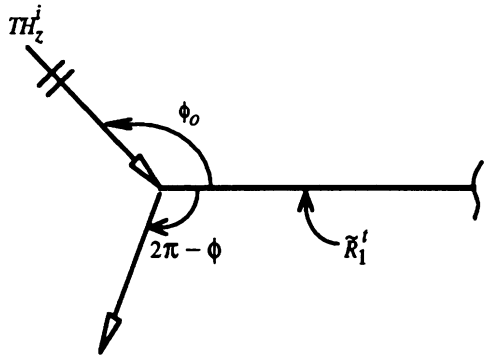

Figure 6: Equivalent problem recovering the transmitted GO field of the structure in Fig. 1.

The far zone diffracted field as predicted by the single half plane models of Fig. 5 is easily computed by using the diffraction coefficient (28). In particular, on superposing the fields generated by the direct and imaged illumination, we obtain the composite diffraction coefficient

$$\begin{aligned} \tilde{S}^{(1)}(\phi,\phi_0) &= \left[D_H(\phi,\phi_0,\tilde{\eta}_1^i) - \Gamma(\sin\phi_0)\, D_H(\phi,2\pi-\phi_0,\tilde{\eta}_1^r)\right] \\ &\quad \cdot e^{-jkd(\sin\phi+\sin\phi_0)}, \\ &\quad 0<\phi<\pi \end{aligned} \tag{39}$$

where $\tilde{\eta}_1^i = 2\tilde{R}_1^i/Z_0$ with $q=d$, $\tilde{\eta}_1^r = 2\tilde{R}_1^r/Z_0$, and D_H is given in (28). This should be compared with the exact diffraction coefficient given in (27).

In the above, we presented a simplified equivalent model which recovers the reflected GO field of the original configuration in Fig. 1. It is not therefore expected that the same resistivities and associated model will also recover the transmitted GO field through the same configuration. Nevertheless, a similar procedure can be employed to construct an equivalent problem which is associated with the same GO field in the $y<0$ region. Such a model is illustrated in Fig. 6, and in order for this model to recover the same GO transmitted field as that associated with the configuration in Fig. 1 we find that the resistivity of the equivalent half plane must be

$$\tilde{R}_1^t = \frac{Z_0}{2}\sin\phi_0\,\frac{\tilde{T}_1^t}{1-\tilde{T}_1^t} \tag{40}$$

where

$$\widetilde{T}_1^t = \frac{T_1}{1 - \Gamma_1 \Gamma e^{-j2kd\sin\phi_0}}. \tag{41}$$

The corresponding diffracted field is given by

$$\widetilde{S}^{(1)}(\phi, \phi_0) = T(\sin\phi_0)\, D_H(\phi, \phi_0, \widetilde{\eta}_1^t)\, e^{-jkd(\sin\phi + \sin\phi_0)} \tag{42}$$

where $\pi < \phi < 2\pi$ and as usual $\widetilde{\eta}_1^t = 2\widetilde{R}_1^t/Z_0$. This diffraction coefficient should be compared with the exact one given by (27).

3 Numerical results

The far field amplitude $S^{(1)}(\phi, \phi_0)$ in (27) was programmed for solution. The numerical factorization routine [9] was used to determine the upper half plane function U_w. As part of the verification of $S^{(1)}(\phi, \phi_0)$, the limit as $R \to \infty$ was taken and the result converged to that of an isolated resistive half plane R_1 as given in (28). Also, by taking the limit $d \to 0$, $S^{(1)}(\phi, \phi_0)$ was found to be in agreement with the material junction result of (29). To complete the verification, the RCS based on the derived diffraction coefficient $S^{(1)}(\phi, \phi_0)$ was compared with data generated by a method of moments implementation of the resistive half plane over resistive plane structure. RCS backscatter results are shown in Fig. 7 for separations of $d = 0.1\lambda$ and 1.0λ with $R = R_1 = Z_0/4$. The moment method data were generated by replacing the resistive half plane and infinite sheet with very wide resistive strips whose resistivity profile after being equal to either R or R_1 was then tapered quadratically to $20Z_0$ over a 60λ section. As seen, the agreement between the numerical and high frequency solutions is excellent. Having validated the high frequency solution, Fig. 8 then shows a characterization of the resistive half plane over the resistive sheet for different separation distances ranging from $d = 0.001\lambda$ to $d = 0.1\lambda$.

To test the validity of the proposed simplified model (see Figs. 5 and 6), the far field amplitudes $\widetilde{S}^{(1)}(\phi, \phi_0)$ in (39) and (42) were programmed as well. Backscatter results in magnitude are shown in Fig. 9 for $d = 0.01\lambda$ with $R = R_1 = Z_0/4$ and for $d = 0.25\lambda$ with $R = Z_0/4$, $R_1 = Z_0/20$. Good agreement is obtained between the magnitudes of the high frequency solutions based on the original and simplified geometries for all angles ϕ, and $d \simeq 0.25\lambda$ was found to be the upper limit of the half plane model. This also holds for bistatic computations except near grazing angles of observation for some values of d. An example of a bistatic pattern is shown in Fig. 10, and it is again verified that the simplified model is a good representation of the original geometry.

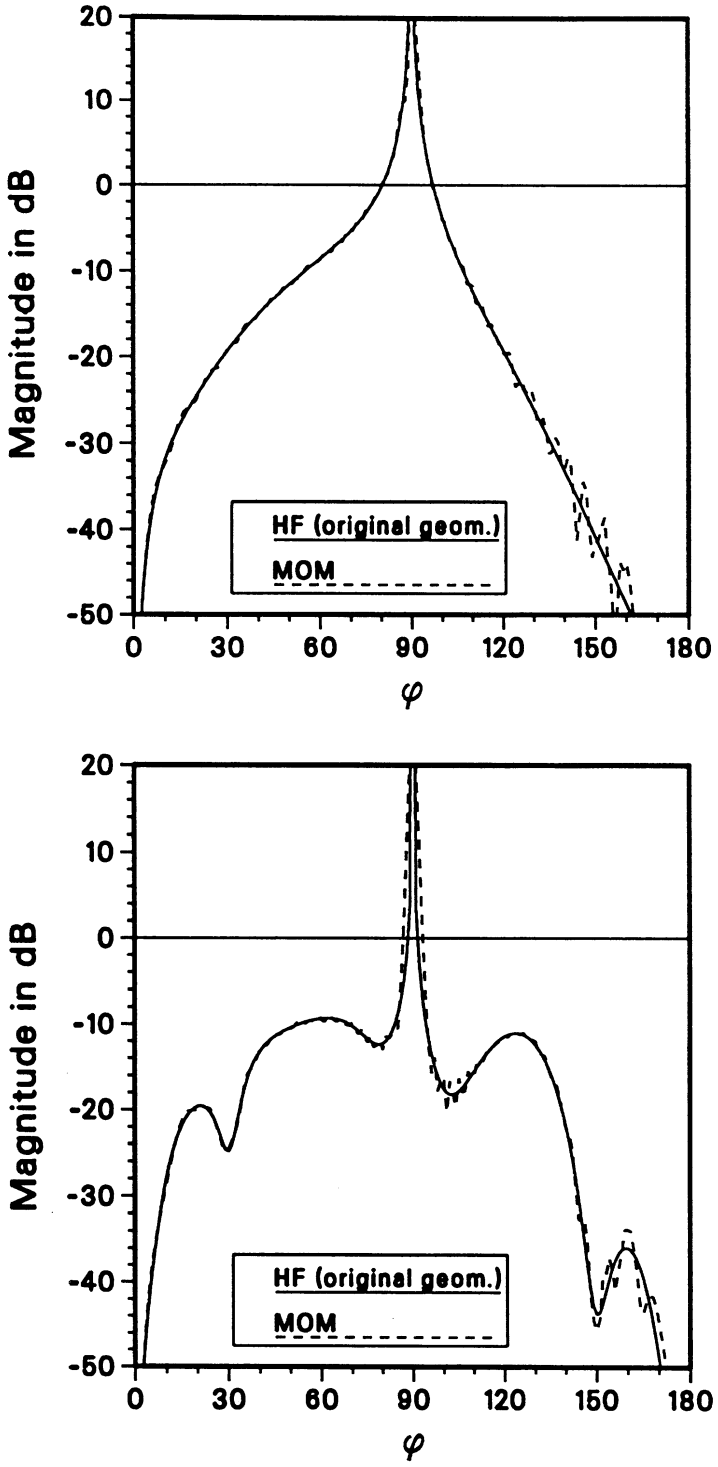

Figure 7: Comparison of backscatter as computed by the moment method and high frequency solutions (of the exact geometry) for the resistive half plane configuration in Fig. 1 with $R = R_1 = Z_0/4$. (a) $d = 0.1\lambda$ (top); (b) $d = 1.0\lambda$ (bottom).

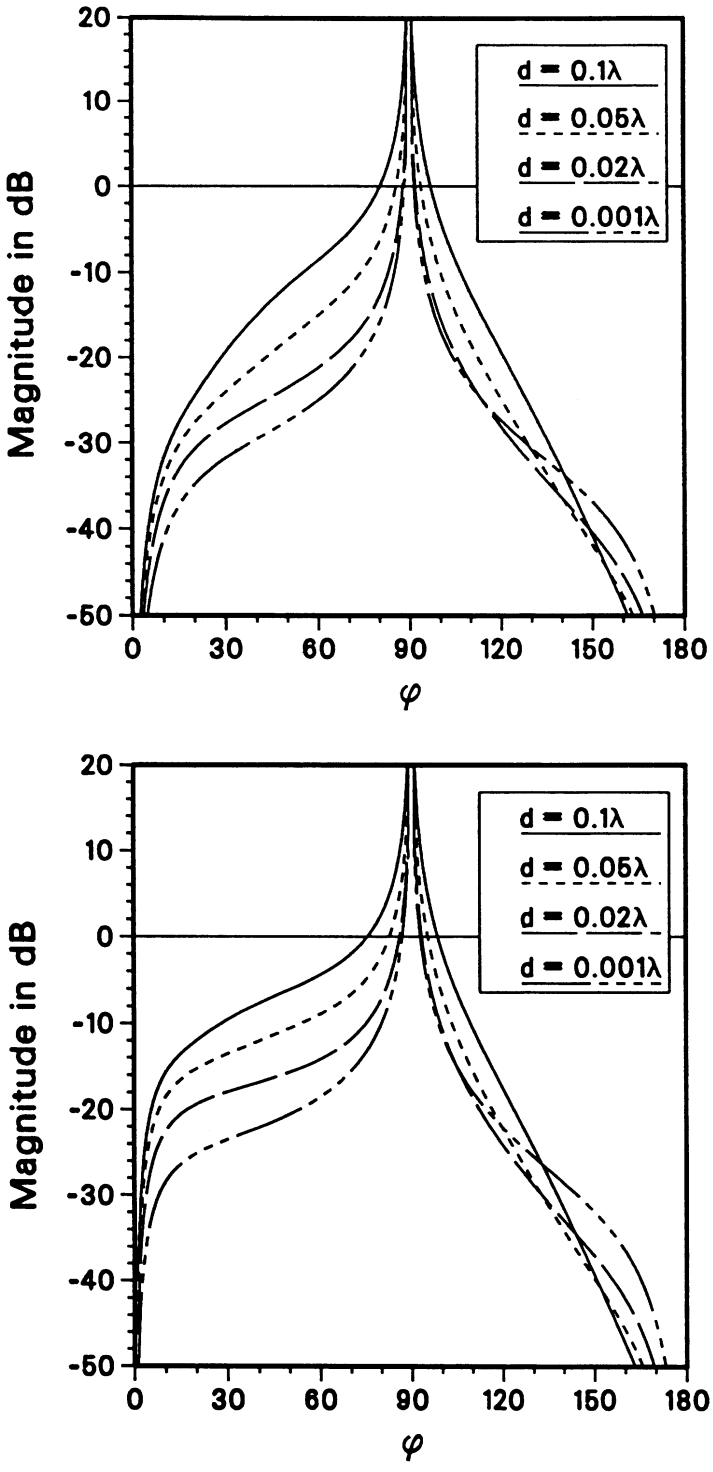

Figure 8: Family of backscatter RCS curves (using the original geometry high frequency solution) of the half plane configuration in Fig. 1 for different separation distances d. (a) $R = R_1 = Z_0/4$ (top); (b) $R = Z_0/4$, $R_1 = Z_0/20$ (bottom).

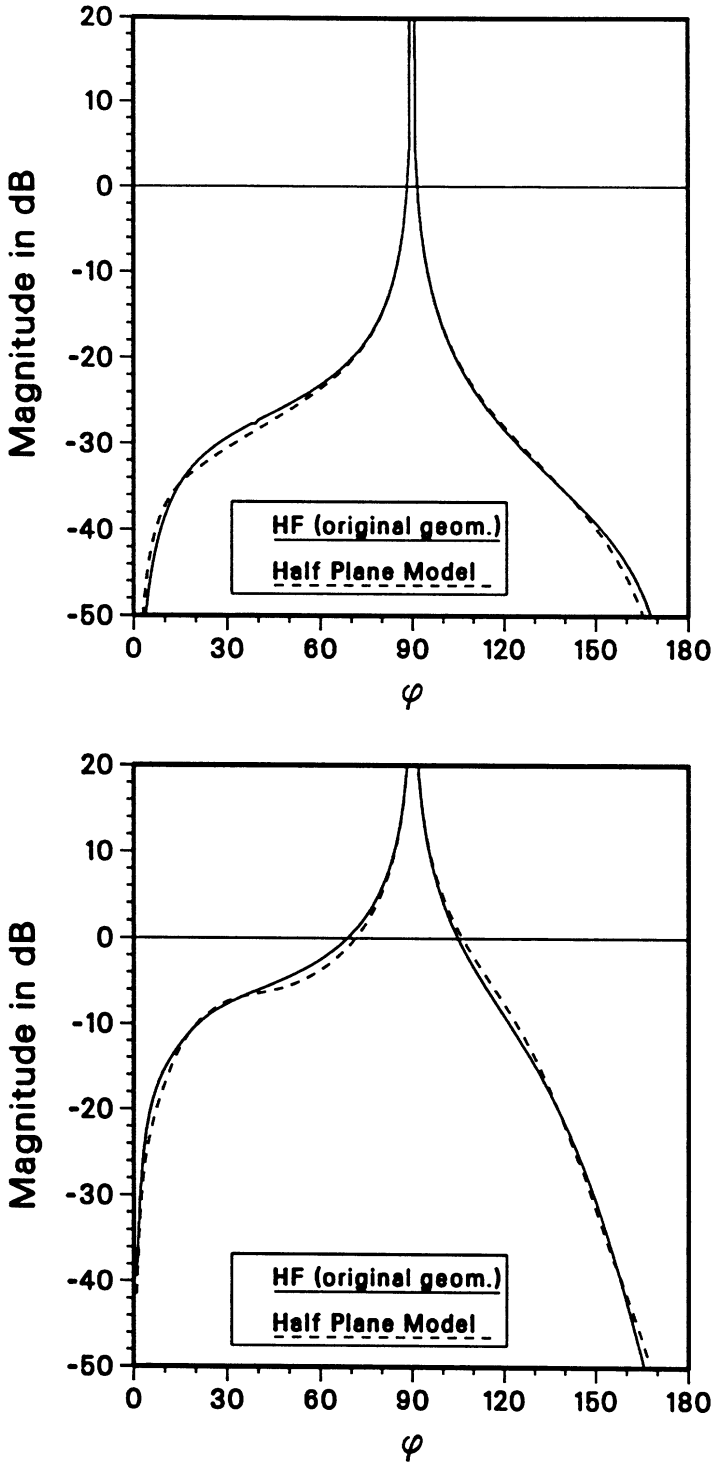

Figure 9: Comparison of backscatter RCS curves based on the original geometry and simplified high frequency solutions for (a) $R = R_1 = Z_0/4$, $d = 0.01\lambda$ (top); (b) $R = Z_0/4$, $R_1 = Z_0/20$, $d = 0.25\lambda$ (bottom).

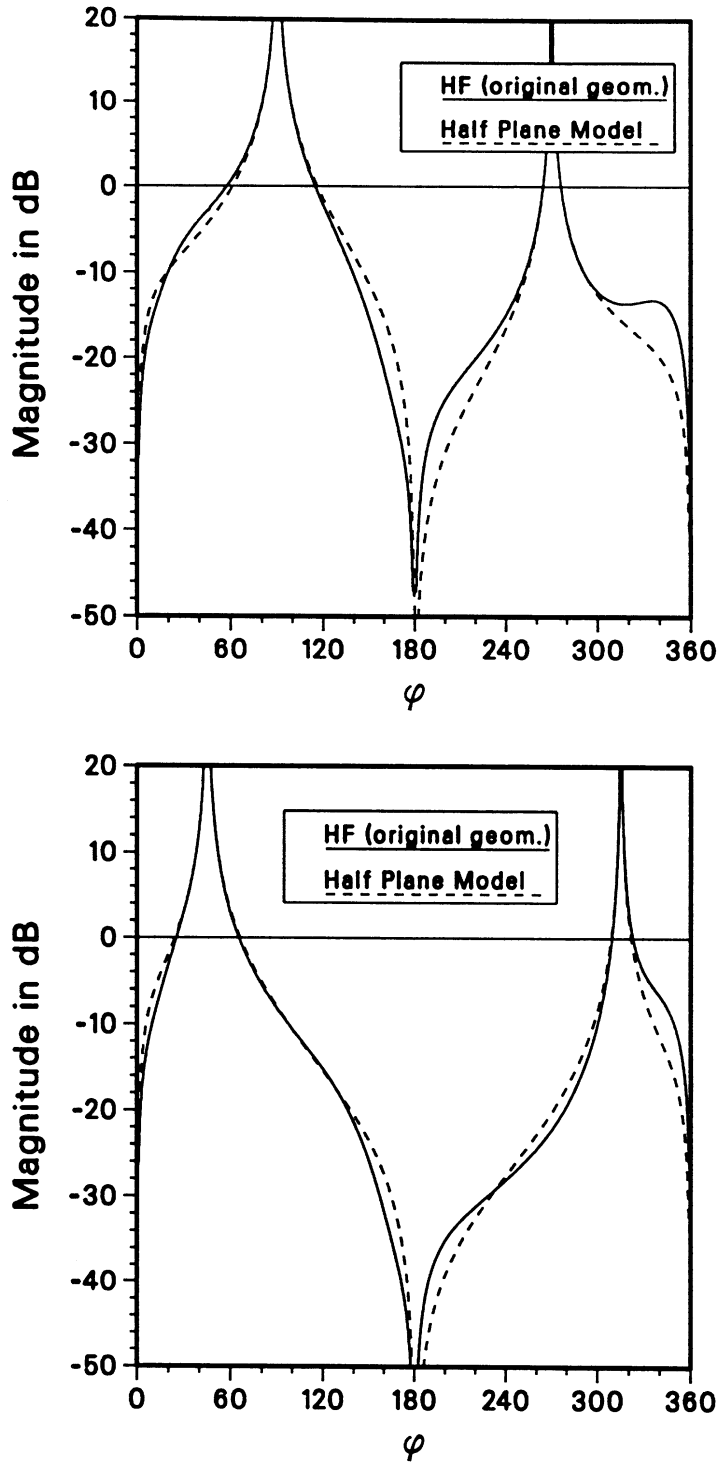

Figure 10: Comparison of bistatic RCS curves based on the original geometry and simplified high frequency solutions for $R = R_1 = Z_0/4$, $d = 0.25\lambda$. (a) $\phi_0 = \pi/2$ (top); (b) $\phi_0 = 3\pi/4$ (bottom).

4 Summary

The exact diffraction coefficient was derived for a resistive half plane over an infinite resistive sheet using the dual integral equation method. An efficient numerical routine was employed to factorize the associated Wiener-Hopf split function. The high frequency solution was found to be in excellent agreement with data generated by a method of moments implementation of the structure, and the results were also verified for the two limiting cases (in the absence of the infinite resistive sheet and when the separation distance between the resistive half plane and sheet goes to zero).

Using the exact solution as a reference, a simplified equivalent model of the structure was developed for the case when the separation of the resistive half plane and sheet is on the order of a tenth of a wavelength or less. The model consisted of a single resistive half plane illuminated with a direct and an image wave equal to the reflected field of the infinite sheet. Good agreement was generally obtained between the high freqeuncy solutions based on the original geometry and the simplified equivalent model for separation distances of up to $d \simeq 0.25\lambda$.

Part II
Characterization of Overlapping Resistive Half Planes

We now turn our attention to the case when the lower resistive sheet in Fig. 1 is truncated at some point $x = W$, $W > 0$, yielding two overlapping resistive half planes as shown in Fig. 11. The dual integral equation method will not provide an exact solution for this configuration since the integral equations obtained in the procedure cannot be decoupled. Therefore, the proposed method of solution is to first consider the field scattered by each edge separately and then develop a higher order diffraction model to account for the interactions between the edges.

A first order diffraction model of the overlapping resistive half planes is the superposition of the diffracted fields from the edge of each resistive half plane in isolation over/under a resistive sheet. The diffracted field from the edge of the upper half plane is given by (27) in Section 1, whereas the diffracted field from the lower half plane edge requires the solution to the inverse problem—the resistive sheet over a resistive half plane—which will be derived in Section 5 below. To develop a higher order diffraction model, we must first obtain the (near zone) fields interacting between the edges of the half planes. The section of the structure between the edges is viewed as a parallel plate waveguide, and we find from an analysis of the scattered field integral equation ([8],[9]) that the incident field couples to waveguide modes. The modes have complex propagation constants associated with the half plane resistivities and the distance separating them. Thus, the modes decay exponentially as they propagate, and upon reaching the opposite end, they reflect back into the waveguide, as well as transmitting or launching a field. Upon deriving coupling, reflection, and launching coefficients for each mode in the parallel plate waveguide, we will obtain a higher order diffraction coefficient of the structure, using transmission line analysis to account for the multiple interactions between the edges due to these modes. There also exist surface waves associated with each half plane which cause additional interactions between the edges, but we find this contribution to the far field scattering can be neglected for the resistivities of concern.

When the separation of the half planes is on the order of a hundreth of a wavelength or less, the structure can be modeled by a simplified planar geometry consisting of a resistive strip inserted between two resistive half planes. The strip insert corresponds to the parallel plate waveguide section of the original structure, and the half planes account for the remaining portions of the original half planes which are not overlapping. The resistivities of this

equivalent structure are determined such that the geometrical optics field of the original one is preserved. The diffraction coefficient for the equivalent simplified model is provided by the program STRIPINS which computes up to third order terms of the diffracted field of the strip [15]. Backscatter and bistatic patterns are presented for various resistivities and separation distances, and good agreement with the higher order diffraction solution is obtained.

5 Resistive sheet over a resistive half plane

Consider now the plane wave (3) incident on a resistive half plane of resistivity R occupying $x < W$ placed a distance d below a planar resistive sheet of resistivity R_1 in the $y = 0$ plane. The boundary conditions for the total fields of the structure are

$$\hat{y} \times \hat{y} \times \bar{E} = -R_1 \hat{y} \times [\bar{H}^+ - \bar{H}^-], \quad y = 0, -\infty < x < \infty \tag{43}$$

$$\hat{y} \times \hat{y} \times \bar{E} = -R \hat{y} \times [\bar{H}^+ - \bar{H}^-], \quad y = -d, x < W \tag{44}$$

in which $\bar{H}^{\pm}$ denotes the total magnetic field above and below the appropriate resistive sheet and $\bar{E}$ is likewise the total electric field. The representation of the total field for this structure is given by (5) in the region $y > 0$ and by (4) when $y < 0$. The reflected and transmitted fields are associated with the resistive sheet of resistivity R_1, leading to the expressions

$$H_z^r = -\Gamma_1(\sin\phi_0)\, e^{jk\rho\cos(\phi+\phi_0)} \tag{45}$$

$$H_z^t = T_1(\sin\phi_0)\, e^{jk\rho\cos(\phi-\phi_0)}, \tag{46}$$

where Γ_1 and T_1 are given in (31).

Referring to (10) as a sum of plane waves emanating from the edge of the half plane at $x = W$, $y = -d$ with the unknown amplitude

$$P(\cos\alpha) e^{jk(W\cos\alpha \mp d\sin\alpha)}, \quad y \gtrless -d,$$

the total scattered field is

$$H_z^s = \int_C T_1(\sin\alpha)\, P(\cos\alpha)\, e^{jk(W\cos\alpha - d\sin\alpha)} e^{-jk\rho\cos(\phi-\alpha)}\, d\alpha \tag{47}$$

for $y > 0$,

$$H_z^s = \int_C \left[e^{-jk\rho\cos(\phi-\alpha)} - \Gamma_1(\sin\alpha)\, e^{-jk\rho\cos(\phi+\alpha)}\right] P(\cos\alpha)\, e^{jk(W\cos\alpha - d\sin\alpha)}\, d\alpha \tag{48}$$

for $-d < y < 0$, and

$$H_z^s = -\int_C \left[e^{jkd\sin\alpha} + \Gamma_1(\sin\alpha)\, e^{-jkd\sin\alpha}\right] P(\cos\alpha)\, e^{jkW\cos\alpha} e^{-jk\rho\cos(\phi+\alpha)}\, d\alpha \tag{49}$$

for $y < -d$, with the contour C defined in Fig. 2*a*.

Applying the boundary conditions for the total field on the $y = -d$ plane, we obtain the dual integral equations

$$\int_{-\infty}^{\infty} Q_1(\lambda) \frac{P(\lambda)}{\sqrt{1-\lambda^2}} e^{-jk(x-W)\lambda}\, d\lambda = \sqrt{1-\lambda_0^2}\, T_1\left(\sqrt{1-\lambda_0^2}\right) e^{-jkd\sqrt{1-\lambda_0^2}}\, e^{jkx\lambda_0},$$
$$x < W$$

$$\int_{-\infty}^{\infty} \frac{P(\lambda)}{\sqrt{1-\lambda^2}} e^{-jk(x-W)\lambda}\, d\lambda = 0\,,\ x > W$$

where $Q_1(\lambda)$ is given in (18) with R interchanged with R_1. Following the dual integral equation solution method given in Section 1, the spectrum $P(\lambda)$ was found to be

$$P(\lambda) = \frac{1}{2\pi j} \frac{\sqrt{1-\lambda^2}\sqrt{1-\lambda_0^2}}{\lambda+\lambda_0} B_1\left(\sqrt{1-\lambda_0^2}\right) \frac{L_{s1}(\lambda)}{L_w(\lambda)} \frac{U_{s1}(-\lambda_0)}{U_w(-\lambda_0)} e^{jkW\lambda_0} \tag{50}$$

where

$$B_1\left(\sqrt{1-\lambda_0^2}\right) = T_1\left(\sqrt{1-\lambda_0^2}\right) e^{-jkd\sqrt{1-\lambda_0^2}}\,, \tag{51}$$

$$U_{s1}(\lambda) = \sqrt{\eta_1}\, \frac{\sqrt{1-\lambda}}{K_+(\lambda, 1/\eta_1)} = L_{s1}(-\lambda)\,, \tag{52}$$

and U_w,L_w are the split functions defined by (21). Given the spectrum in (50), the integrals (47) and (49) are evaluated by the steepest descent method, and following the definition of the far zone scattered field in (26), the diffraction coefficient of the resistive sheet over the resistive half plane is

$$S^{(2)}(\phi,\phi_0) = \frac{e^{-j\frac{\pi}{4}}}{\sqrt{2\pi k}} \left\{ \begin{matrix} B_1(\sin\phi) \\ A_1(-\sin\phi)\, e^{-jkd\sin\phi} \end{matrix} \right\} B_1(\sin\phi_0) \frac{\sin\phi\sin\phi_0}{\cos\phi+\cos\phi_0}$$
$$\cdot \frac{L_{s1}(\cos\phi)\, L_{s1}(\cos\phi_0)}{L_w(\cos\phi)\, L_w(\cos\phi_0)} e^{jkW(\cos\phi+\cos\phi_0)} \tag{53}$$

for $\left\{ \begin{matrix} 0 < \phi < \pi \\ \pi < \phi < 2\pi \end{matrix} \right\}$, where A_1 is given in (19) with Γ replaced by Γ_1.

6 Higher order diffraction model

The overlapping resistive half plane structure is defined by a half plane of resistivity R_1 located at $y = 0$, $x > 0$ positioned above a half plane of

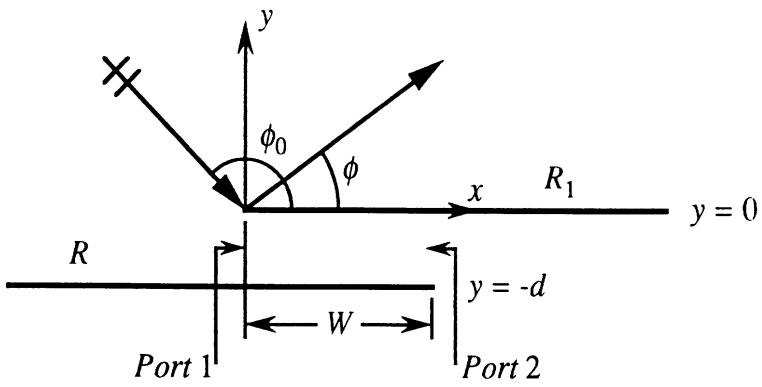

Figure 11: Geometry of the overlapping resistive half planes.

resistivity R at $y = -d$, $x < W$, $(W > 0)$, as shown in Fig. 11. Combining the results of Sections 1 and 5, the first order far zone scattered field of the overlapping resistive half planes is

$$H_z^s \simeq \frac{e^{-jk\rho}}{\sqrt{\rho}} S^{(3)}(\phi, \phi_0)$$

where

$$S^{(3)}(\phi, \phi_0) = S^{(1)}(\phi, \phi_0) + S^{(2)}(\phi, \phi_0) \tag{54}$$

is the diffraction coefficient of the structure with $S^{(1)}$ given in (27) and $S^{(2)}$ given in (53). For large resistivities, large overlap widths and small separations, this first order model is sufficiently accurate in predicting the scattered far field, since the edges of the half planes do not interact. However, we would like to develop a general model that can handle considerably small overlap widths, which requires an investigation of the near fields interacting between the edges of the half planes. Viewing the section $0 < x < W$, $-d < y < 0$ as a parallel plate waveguide, a transmission line analysis can be applied upon finding the coupled modes and pertinent reflection and launching coefficients.

6.1 Mode coupling

We first seek to find the field coupled to the waveguide section at the opening $x = 0$, $-d < y < 0$, defined in Fig. 11 as port 1. Using the solution to the resistive half plane over the resistive sheet for the analysis of the field coupled

at port 1, the integral equation of the scattered field within the waveguide ($x > 0$, $-d < y < 0$) is obtained from (12) with $\lambda = \cos\alpha$:

$$H_z^s = -\int_{-\infty}^{\infty} \left[e^{jky\sqrt{1-\lambda^2}} - \Gamma(\sqrt{1-\lambda^2})\, e^{-jk(y+2d)\sqrt{1-\lambda^2}} \right] \frac{P^{(1)}(\lambda)}{\sqrt{1-\lambda^2}}\, e^{-jkx\lambda}\, d\lambda \tag{55}$$

where $P^{(1)}(\lambda) = P(\lambda)$ in (25). Since this integral equation is to be evaluated only for $x > 0$, the contour can be closed in the lower λ-plane, to re-express (55) by a sum of pole residues and branch cut contributions. The evaluation of the integral over the branch cut (shown in Fig. 2*b*) gives a surface wave field associated with the resistive half plane. We find that for the resistivities of concern, this contribution is small compared to that of the dominant waveguide mode and will therefore be neglected. For the captured poles, the residues are collected at $\lambda = \lambda_n$, the zeros of $U_w(\lambda)$, producing the field

$$H_z^{res} = \sum_{n=1}^{\infty} C_n^{(1)}(\lambda_0) \left[e^{jky\sqrt{1-\lambda_n^2}} - \Gamma\left(\sqrt{1-\lambda_n^2}\right) e^{-jk(y+2d)\sqrt{1-\lambda_n^2}} \right] e^{-jkx\lambda_n} \tag{56}$$

where we have defined

$$C_n^{(1)}(\lambda_0) = -\frac{\sqrt{1-\lambda_0^2}}{\lambda_n + \lambda_0} A\left(\sqrt{1-\lambda_0^2}\right) \frac{U_{s1}(\lambda_n)\, U_{s1}(\lambda_0)}{U_w'(\lambda_n)\, U_w(\lambda_0)} \tag{57}$$

as the coupling coefficient of the incident field to the n^{th} mode at port 1 with

$$\begin{aligned} U_w'(\lambda_n) &= \left.\frac{dU_w(\lambda)}{d\lambda}\right|_{\lambda=\lambda_n} \\ &= -\frac{\lambda_n}{L_w(\lambda_n)} \left[2 + \frac{\eta_1 + \eta}{\sqrt{1-\lambda_n^2}} - 2\left(1 - jkd\sqrt{1-\lambda_n^2}\right) e^{-j2kd\sqrt{1-\lambda_n^2}} \right] . \end{aligned}$$

The summed fields in (56) correspond to waveguide modes propagating and decaying exponentially in the positive x direction, requiring that the zeros of $U_w(\lambda)$ lie only in the fourth quadrant of the complex λ-plane. This was verified by determining the first five zeros (closest to the origin) using a numerical search routine, and the zeros λ_1 corresponding to the dominant mode are listed in Table 1 for several η, η_1, and d. Since the resistive half plane and sheet form a penetrable waveguide, another condition to ensure proper modes is that they decay away from the structure in the $\pm y$ directions. Referring to the scattered field expressions in (11) and (13), this condition is met when $\mathrm{Im}\left(\sqrt{1-\lambda_n^2}\right) < 0$, requiring the particular branch cut shown in Fig. 2*b* such that the zeros λ_n lie to the right of the branch in the lower λ-plane.

η	η_1	d/λ	λ_1
0.5	0.5	0.1	(1.0021581,-0.4706920)
		0.01	(2.1109666,-2.0023438)
		0.001	(6.3453235,-6.3947592)
0.1	0.5	0.1	(0.9622725,-0.2955593)
		0.01	(1.6968256,-1.5045357)
		0.001	(4.9344730,-4.9452179)
0.1	0.1	0.1	(0.9956063,-0.0869338)
		0.01	(1.1930695,-0.6856712)
		0.001	(2.9100025,-2.7588511)

Table 1: Zeros of $U_w(\lambda)$ corresponding to the dominant modes.

Considering next the field coupled to the waveguide section at port 2, the substitution $\lambda = \cos\alpha$ in (48) gives the scattered field integral equation

$$H_z^s = \int_{-\infty}^{\infty} \left[e^{-jk(y+d)\sqrt{1-\lambda^2}} - \Gamma_1(\sqrt{1-\lambda^2})\, e^{jk(y-d)\sqrt{1-\lambda^2}} \right] \cdot \frac{P^{(2)}(\lambda)}{\sqrt{1-\lambda^2}}\, e^{-jk(x-W)\lambda}\, d\lambda \tag{58}$$

for $-d < y < 0$, where $P^{(2)}(\lambda) = P(\lambda)$ in (50). Closing the contour in the upper λ-plane and retaining only the contribution of the residues at $\lambda = -\lambda_n$, the waveguide modes propagating in the negative x direction from port 2 are summed as

$$H_z^{res} = \sum_{n=1}^{\infty} C_n^{(2)}(\lambda_0) \left[e^{-jk(y+d)\sqrt{1-\lambda_n^2}} - \Gamma_1\left(\sqrt{1-\lambda_n^2}\right) e^{jk(y-d)\sqrt{1-\lambda_n^2}} \right] e^{jk(x-W)\lambda_n} \tag{59}$$

where we have defined

$$C_n^{(2)}(\lambda_0) = -\frac{\sqrt{1-\lambda_0^2}}{\lambda_n - \lambda_0} B_1\left(\sqrt{1-\lambda_0^2}\right) \frac{U_{s1}(\lambda_n)\, L_{s1}(\lambda_0)}{U_w'(\lambda_n)\, L_w(\lambda_0)}\, e^{jkW\lambda_0} \tag{60}$$

as the coupling coefficient of port 2.

6.2 Reflection and launching coefficients

As the coupled fields (56) and (59) impinge upon the opposite ports, the scattered field can be represented by (47) through (49) and (11) through (13), respectively, and we are concerned only with the fields reflected back into the waveguide and those launched to the far zone. Therefore new spectral functions need to be derived for these scattered fields, which is accomplished

by applying the dual integral equation method with the coupled modes as the incident fields.

From (56) the n^{th} waveguide mode incident on port 2 arising from the field coupled at port 1 is of the form

$$H_{zn}^{i} = \left[e^{jky\sqrt{1-\lambda_n^2}} - \Gamma\left(\sqrt{1-\lambda_n^2}\right) e^{-jk(y+2d)\sqrt{1-\lambda_n^2}}\right] e^{-jkx\lambda_n} \tag{61}$$

for $-d < y < 0$. Applying the boundary conditions of the total field in the $y = -d$ plane, we obtain the dual integral equations

$$\int_{-\infty}^{\infty} Q_1(\lambda) \frac{P_n^{(2)}(\lambda)}{\sqrt{1-\lambda^2}} e^{-jk(x-W)\lambda}\, d\lambda = 0\,,\ x < W$$

$$\int_{-\infty}^{\infty} \frac{P_n^{(2)}(\lambda)}{\sqrt{1-\lambda^2}} e^{-jk(x-W)\lambda}\, d\lambda = \Gamma\left(\sqrt{1-\lambda_n^2}\right) e^{-jkd\sqrt{1-\lambda_n^2}}\, e^{-jkx\lambda_n}\,,\ x > W.$$

Following the procedure of Section 1, the spectra for the n^{th} incident waveguide mode was determined to be

$$P_n^{(2)}(\lambda) = -\frac{1}{2\pi j} \frac{\sqrt{1-\lambda^2}}{\lambda - \lambda_n} \Gamma\left(\sqrt{1-\lambda_n^2}\right) \frac{L_{s1}(\lambda)}{L_w(\lambda)} \frac{L_w(\lambda_n)}{L_{s1}(\lambda_n)} e^{-jkd\sqrt{1-\lambda_n^2}} e^{-jkW\lambda_n}\,. \tag{62}$$

To find the field reflected back into the waveguide, we use (58) with $P^{(2)}(\lambda) = P_n^{(2)}(\lambda)$, and upon closing the contour in the upper λ-plane and collecting the residues at $\lambda = -\lambda_m$,

$$H_{zn}^{res} = \sum_{m=1}^{\infty} \Gamma_{mn}^{(2)} \left[e^{-jk(y+d)\sqrt{1-\lambda_m^2}} - \Gamma_1\left(\sqrt{1-\lambda_m^2}\right) e^{jk(y-d)\sqrt{1-\lambda_m^2}}\right] e^{jk(x-W)\lambda_m} \tag{63}$$

where we have defined

$$\Gamma_{mn}^{(2)} = \frac{\Gamma\left(\sqrt{1-\lambda_n^2}\right)}{\lambda_m + \lambda_n} \frac{U_{s1}(\lambda_m)\, L_w(\lambda_n)}{U_w'(\lambda_m)\, L_{s1}(\lambda_n)} e^{-jkd\sqrt{1-\lambda_n^2}}\, e^{-jkW\lambda_n} \tag{64}$$

as the modal reflection coefficient of the n^{th} waveguide mode coupled to the m^{th} reflected mode at port 2. The reflected fields of (63) have the same spatial dependence as the coupled fields of port 2 (see (59)). Again, the branch cut contribution is assumed to be negligible. To find the field launched from port 2 due to the incident field (61), we evaluate the integrals (47) and (49) by the steepest descent method after substituting $P(\cos\alpha) = P_n^{(2)}(\cos\alpha)$, which yields the launching coefficient

$$L_n^{(2)}(\phi) = -\frac{e^{-j\frac{\pi}{4}}}{\sqrt{2\pi k}} \left\{ \begin{matrix} B_1(\sin\phi) \\ A_1(-\sin\phi)\, e^{-jkd\sin\phi} \end{matrix} \right\} \Gamma\left(\sqrt{1-\lambda_n^2}\right) \frac{\sin\phi}{\cos\phi - \lambda_n}$$
$$\cdot \frac{L_{s1}(\cos\phi)\, L_w(\lambda_n)}{L_w(\cos\phi)\, L_{s1}(\lambda_n)} e^{-jkd\sqrt{1-\lambda_n^2}}\, e^{jkW(\cos\phi - \lambda_n)} \tag{65}$$

for $\left\{\begin{array}{l} 0<\phi<\pi \\ \pi<\phi<2\pi \end{array}\right\}$.

Likewise we consider the n^{th} waveguide mode incident on port 1 arising from the field coupled at port 2, which from (59) has the form

$$H_{zn}^{i} = \left[e^{jk(y+d)\sqrt{1-\lambda_n^2}} - \Gamma_1\left(\sqrt{1-\lambda_n^2}\right) e^{jk(y-d)\sqrt{1-\lambda_n^2}}\right] e^{jk(x-W)\lambda_n} \tag{66}$$

valid for $-d<y<0$. Applying the boundary conditions in the $y=0$ plane, we obtain the dual integral equations

$$\int_{-\infty}^{\infty} \frac{P_n^{(1)}(\lambda)}{\sqrt{1-\lambda^2}}\, e^{-jkx\lambda}\, d\lambda = \Gamma_1\left(\sqrt{1-\lambda_n^2}\right) e^{-jkd\sqrt{1-\lambda_n^2}} e^{jk(x-W)\lambda_n}\ ,\ x<0$$

$$\int_{-\infty}^{\infty} Q(\lambda)\, \frac{P_n^{(1)}(\lambda)}{\sqrt{1-\lambda^2}}\, e^{-jkx\lambda}\, d\lambda = 0\ ,\ x>0,$$

which are satisfied by the spectral function

$$P_n^{(1)}(\lambda) = \frac{1}{2\pi j}\, \frac{\sqrt{1-\lambda^2}}{\lambda+\lambda_n}\, \Gamma_1\left(\sqrt{1-\lambda_n^2}\right) \frac{U_s(\lambda)}{U_w(\lambda)}\, \frac{U_w(-\lambda_n)}{U_s(-\lambda_n)}\, e^{-jkd\sqrt{1-\lambda_n^2}}\, e^{-jkW\lambda_n}\ . \tag{67}$$

The field reflected back into the waveguide is determined by substituting $P^{(1)}(\lambda) = P_n^{(1)}(\lambda)$ into (55) and closing the contour in the lower λ-plane. Collecting the residues at $\lambda = \lambda_m$ gives

$$H_{zn}^{res} = \sum_{m=1}^{\infty} \Gamma_{mn}^{(1)} \left[e^{jky\sqrt{1-\lambda_m^2}} - \Gamma\left(\sqrt{1-\lambda_m^2}\right) e^{-jk(y+2d)\sqrt{1-\lambda_m^2}}\right] e^{-jkx\lambda_m} \tag{68}$$

where

$$\Gamma_{mn}^{(1)} = \frac{\Gamma_1\left(\sqrt{1-\lambda_n^2}\right)}{\lambda_m+\lambda_n}\, \frac{U_s(\lambda_m)\, L_w(\lambda_n)}{U_w'(\lambda_m)\, L_s(\lambda_n)}\, e^{-jkd\sqrt{1-\lambda_n^2}}\, e^{-jkW\lambda_n} \tag{69}$$

is the modal reflection coefficient associated with port 1, and (68) has the same spatial dependence as the coupled fields at port 1 in (56). We also note that $\Gamma_{mn}^{(1)} = \Gamma_{mn}^{(2)}$ when $R_1 = R$. The coefficient of far zone field launched from port 1 is derived from applying the steepest descent method to the integrals (11) and (13) after the substitution $P(\cos\alpha) = P_n^{(1)}(\cos\alpha)$, resulting in

$$L_n^{(1)}(\phi) = \frac{e^{-j\frac{\pi}{4}}}{\sqrt{2\pi k}} \left\{\begin{array}{l} A(\sin\phi) \\ B(-\sin\phi)\, e^{-jkd\sin\phi} \end{array}\right\} \Gamma_1\left(\sqrt{1-\lambda_n^2}\right)\, \frac{\sin\phi}{\cos\phi+\lambda_n}$$
$$\cdot \frac{U_s(\cos\phi)\, L_w(\lambda_n)}{U_w(\cos\phi)\, L_s(\lambda_n)}\, e^{-jkd\sqrt{1-\lambda_n^2}}\, e^{-jkW\lambda_n} \tag{70}$$

for $\left\{\begin{array}{l} 0<\phi<\pi \\ \pi<\phi<2\pi \end{array}\right\}$.

6.3 Multiply diffracted field

From the results above we observe that the diffracted field of each coupled mode is comprised of the field launched from the opposite port and the reflected field launched upon its return. Adding these doubly and triply diffracted field terms to (54), the diffraction coefficient of the overlapping resistive half planes becomes

$$\begin{aligned} S^{(3)}(\phi,\phi_0) = {} & S^{(1)}(\phi,\phi_0) + S^{(2)}(\phi,\phi_0) \\ & + \sum_{n=1}^{\infty} \Bigg\{ C_n^{(1)}(\phi_0) \left[L_n^{(2)}(\phi) + \sum_{m=1}^{\infty} \Gamma_{mn}^{(2)} L_m^{(1)}(\phi) \right] \\ & \quad + C_n^{(2)}(\phi_0) \left[L_n^{(1)}(\phi) + \sum_{m=1}^{\infty} \Gamma_{mn}^{(1)} L_m^{(2)}(\phi) \right] \Bigg\} \end{aligned} \tag{71}$$

where $C_n^{(1),(2)}$ are given in (57) and (60), $\Gamma_{mn}^{(1),(2)}$ are given in (69) and (64), and $L_n^{(1),(2)}$ are given in (70) and (65). Using transmission line analysis, the summation of diffraction terms can be carried out indefinitely, accounting for all of the interactions between the edges of the half planes due to modal fields. Since the waveguide is lossy, the modes $n > 1$ decay rapidly for the resistivities of concern ($R, R_1 > Z_0/40$) and give negligible contribution to the far field. Thus only the dominant mode $n = 1$ needs to be considered for the higher order diffraction terms. The diffraction coefficient in (71) is then

$$\begin{aligned} S^{(3)}(\phi,\phi_0) = {} & S^{(1)}(\phi,\phi_0) + S^{(2)}(\phi,\phi_0) \\ & + \left\{ C_1^{(1)}(\phi_0) \left[L_1^{(2)}(\phi) + \Gamma_{11}^{(2)} L_1^{(1)}(\phi) \right] \right. \\ & \quad \left. + C_1^{(2)}(\phi_0) \left[L_1^{(1)}(\phi) + \Gamma_{11}^{(1)} L_1^{(2)}(\phi) \right] \right\} \\ & \cdot \left[1 + \Gamma_{11}^{(1)}\Gamma_{11}^{(2)} + \left(\Gamma_{11}^{(1)}\Gamma_{11}^{(2)} \right)^2 + \cdots \right] , \end{aligned}$$

and since $|\Gamma_{11}^{(1)}|, |\Gamma_{11}^{(2)}| < 1$, the infinite series can be replaced with its asymptotic value, giving

$$\begin{aligned} S^{(3)}(\phi,\phi_0) = {} & S^{(1)}(\phi,\phi_0) + S^{(2)}(\phi,\phi_0) \\ & + \left\{ C_1^{(1)}(\phi_0) \left[L_1^{(2)}(\phi) + \Gamma_{11}^{(2)} L_1^{(1)}(\phi) \right] \right. \\ & \quad \left. + C_1^{(2)}(\phi_0) \left[L_1^{(1)}(\phi) + \Gamma_{11}^{(1)} L_1^{(2)}(\phi) \right] \right\} \\ & \cdot \left[1 - \Gamma_{11}^{(1)}\Gamma_{11}^{(2)} \right]^{-1} \end{aligned} \tag{72}$$

as the dominant mode diffraction coefficient of the overlapping resistive half planes.

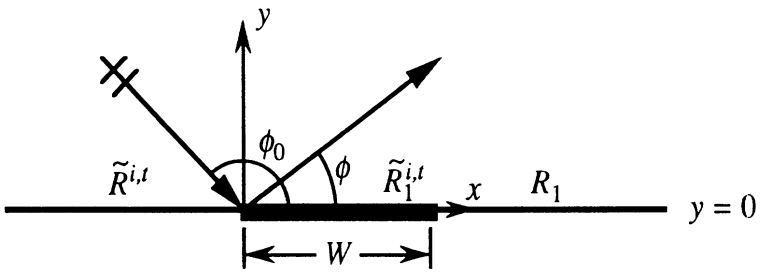

Figure 12: Equivalent geometry recovering the GO field of the original structure in Fig. 11.

7 Simplified model for small d

When the separation d between the overlapping resistive half planes is small, $kd \ll 1$, the structure is virtually planar and can be modeled by a resistive strip inserted between two resistive half planes. This equivalent geometry of the structure is shown in Fig. 12, where the lower half plane has been effectively transfered to the $y = 0$ plane. The equivalent resistivities $\tilde{R}^{i,t}$ and $\tilde{R}_1^{i,t}$ must be determined such that the geometrical optics (GO) fields of the original structure are preserved. For the waveguide section $0 < x < W$ in Fig. 11, the reflected field is that of two parallel resistive sheets and is given in (30) of Section 2. For the equivalent resistive strip, then, we obtain

$$\tilde{R}_1^i = -\frac{Z_0}{2} \sin\phi_0 \frac{1 + \tilde{\Gamma}_1^i}{\tilde{\Gamma}_1^i}, \tag{73}$$

where

$$\tilde{\Gamma}_1^i = \Gamma_1 + \frac{T_1^2 \Gamma\, e^{-j2kd\sin\phi_0}}{1 - \Gamma_1 \Gamma\, e^{-j2kd\sin\phi_0}}. \tag{74}$$

For the equivalent resistive half plane $x < 0$ in Fig. 12, the reflected field of the original geometry is given in (6), and it follows that its equivalent resistivity is simply

$$\tilde{R}^i = -\frac{Z_0}{2} \sin\phi_0 \left[1 + \frac{1}{\Gamma} e^{j2kd\sin\phi_0}\right]. \tag{75}$$

In the case of the transmitted field, the same equivalent geometry is applicable, though different equivalent resistivities are required than those for the reflected field case. In order for the model to recover the same GO transmitted field as the original structure, we find that for the equivalent resistive strip

$$\tilde{R}_1^t = \frac{Z_0}{2} \sin\phi_0 \frac{\tilde{T}_1^t}{1 - \tilde{T}_1^t}, \tag{76}$$

where

$$\tilde{T}_1^t = \frac{T_1 T}{1 - \Gamma_1 \Gamma\, e^{-j2kd\sin\phi_0}}. \tag{77}$$

The transmitted field of the equivalent resistive half plane $x < 0$ must be equivalent to (7), requiring that its resistivity is

$$\tilde{R}^t = R. \tag{78}$$

In the limit as d approaches zero, the equivalent resistivities become

$$\tilde{R}_1^i = \tilde{R}_1^t = \frac{R_1 R}{R_1 + R}, \qquad \tilde{R}^i = \tilde{R}^t = R$$

for all y as expected.

The program STRIPINS computes the E-polarized diffraction by a resistive strip inserted between two resistive half planes, accounting for the singly, doubly and triply diffracted fields associated with the strip for aspects of $0 < \phi, \phi_0 < \pi$ [15]. We denote the diffraction coefficient generated by this code as $D_E(\phi, \phi_0, \eta_l, \eta_s, \eta_r, W)$, where $\eta_{l,r}$ are the normalized surface impedances of the left and right hand half planes and η_s is the normalized surface impedance of the strip insert of width W. Using duality, the diffraction coefficient of the equivalent geometry in Fig. 12 under H-polarized illumination is then

$$\tilde{S}^{(3)}(\phi, \phi_0) = D_E(\phi, \phi_0, 1/\tilde{\eta}^i, 1/\tilde{\eta}_1^i, 1/\eta_1, W) \tag{79}$$

for $0 < \phi < \pi$, and

$$\tilde{S}^{(3)}(\phi, \phi_0) = -D_E(2\pi - \phi, \phi_0, 1/\eta, 1/\tilde{\eta}_1^t, 1/\eta_1, W) \tag{80}$$

for $\pi < \phi < 2\pi$, where, referring to (73) through (77), $\tilde{\eta}_1^{i,t} = 2\tilde{R}_1^{i,t}/Z_0$ and $\tilde{\eta}^i = 2\tilde{R}^i/Z_0$. This diffraction coefficient should be compared to the one for the higher order diffraction model given in (72).

8 Numerical results and discussion

To check the validity of the assumption that the branch cut contributions in (55) and (58) are negligible, the currents on the upper resistive half plane due

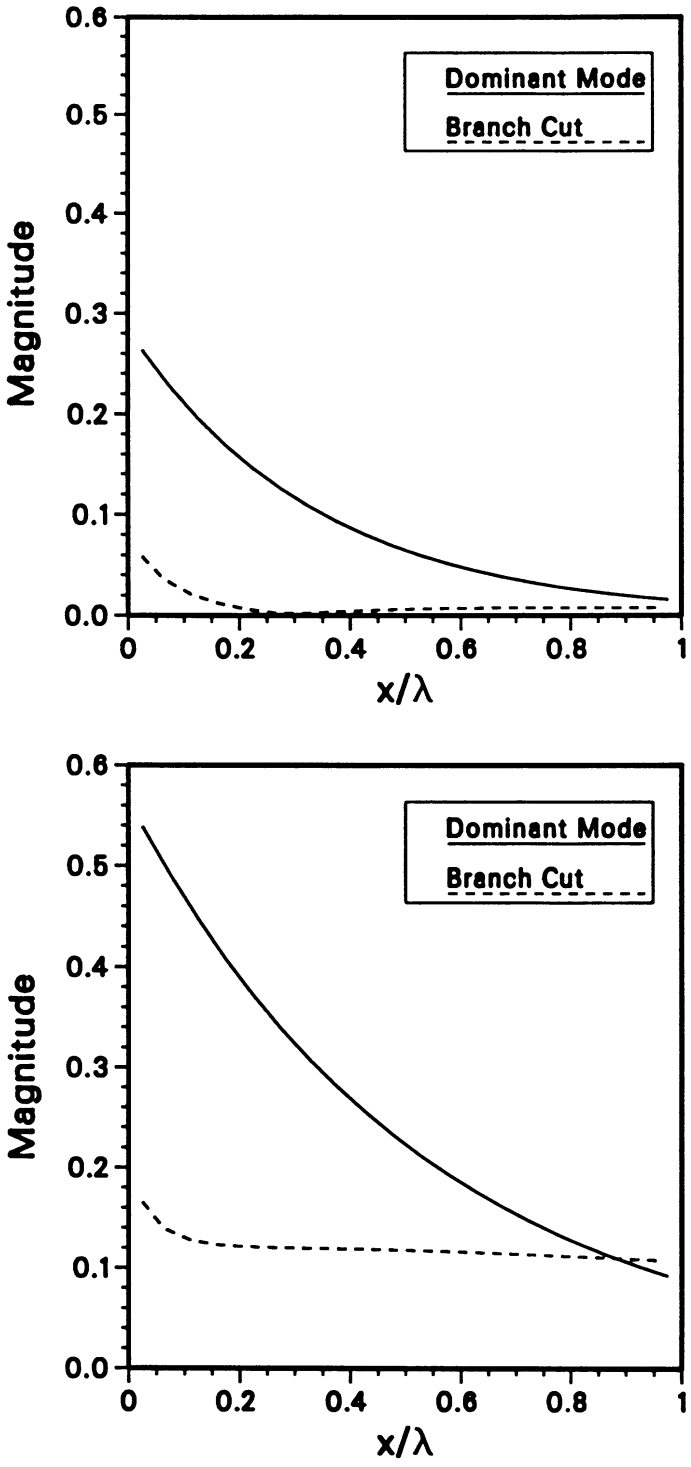

Figure 13: Magnitude of current on the resistive half plane of Fig. 1 with $d = 0.1\lambda$, $\phi_0 = \pi/18$, and $R = Z_0/4$. (a) $R_1 = Z_0/4$ (top); (b) $R_1 = Z_0/20$ (bottom).

to the dominant mode field and the branch cut contribution were generated. Results are shown in Fig. 13 for $R_1 = Z_0/4$ and $Z_0/20$, with $d = 0.1\lambda$, $\phi_0 = \pi/18$, $R = Z_0/4$, where the branch cut current was computed by a numerical integration of (55) over the branch cut in the lower λ-plane. The magnitude of the dominant mode current is indeed much greater than the branch cut current for most R, R_1 and would therefore have a greater contribution to the higher order diffracted field. However, Fig. 13*b* indicates that for $R_1 \ll R$ the branch cut contribution is on the order of the dominant mode contribution and would have to be accounted for in the higher order diffraction model.

The far field amplitude $S^{(3)}(\phi, \phi_0)$ in (72) was computed using the numerical factorization routine in [9] to determine the necessary split functions. To verify the higher order diffraction model, the results were compared with data generated by a method of moments implementation of the overlapping resistive half planes. RCS backscatter results are given in Fig. 14 for the dimensions $d = 0.1\lambda$, $W = 0.5\lambda$ and $d = 0.05\lambda$, $W = 0.1\lambda$ with $R = R_1 = Z_0/4$, showing very good agreement. We point out that the lobe in Fig. 14*a* arises from the launching of the modal fields, which is accounted for in the diffraction model by the higher order terms in (72).

To test the validity of the simplified equivalent model shown in Fig. 12, the STRIPINS code was utilized to compute the far field amplitude $\tilde{S}^{(3)}$ in (79) and (80). Backscatter results are compared to (72) in Fig. 15 for the dimensions of $d = 0.01\lambda$, $W = 0.2\lambda$ and $d = 0.001\lambda$, $W = 0.15\lambda$ with $R = R_1 = Z_0/4$. Good agreement is obtained between the two models, given the limitations on the STRIPINS model of $d \lesssim 0.01\lambda$ and $W \gtrsim 0.15\lambda$. This very small limit on the separation d is expected because of the limitation on effectively modeling the edges of the half planes. In the original geometry the edge at $x = 0$ is much more distinct than the edge at $x = W$ for $0 < \phi_0 < \pi$, whereas in the simplified geometry both edges are modeled by material junctions having the same scattering characteristics. Also, for grazing aspects of incidence and observation (where any guided modes are the dominant contributors), the STRIPINS model cannot account for these effects. From Table 1 it is seen that only for very small separations the dominant modes are largely attenuated, and thus the STRIPINS model is restricted to those cases. The lower limit on W is due to the accuracy of the STRIPINS code for small W. These same limitations apply for bistatic results as well, and two patterns are shown in Fig. 16 for $\phi_0 = \pi/4$ and $\phi_0 = 3\pi/4$. Good agreement with the higher order diffraction model is again obtained, verifying that the simplified model is a good representation of the original structure.

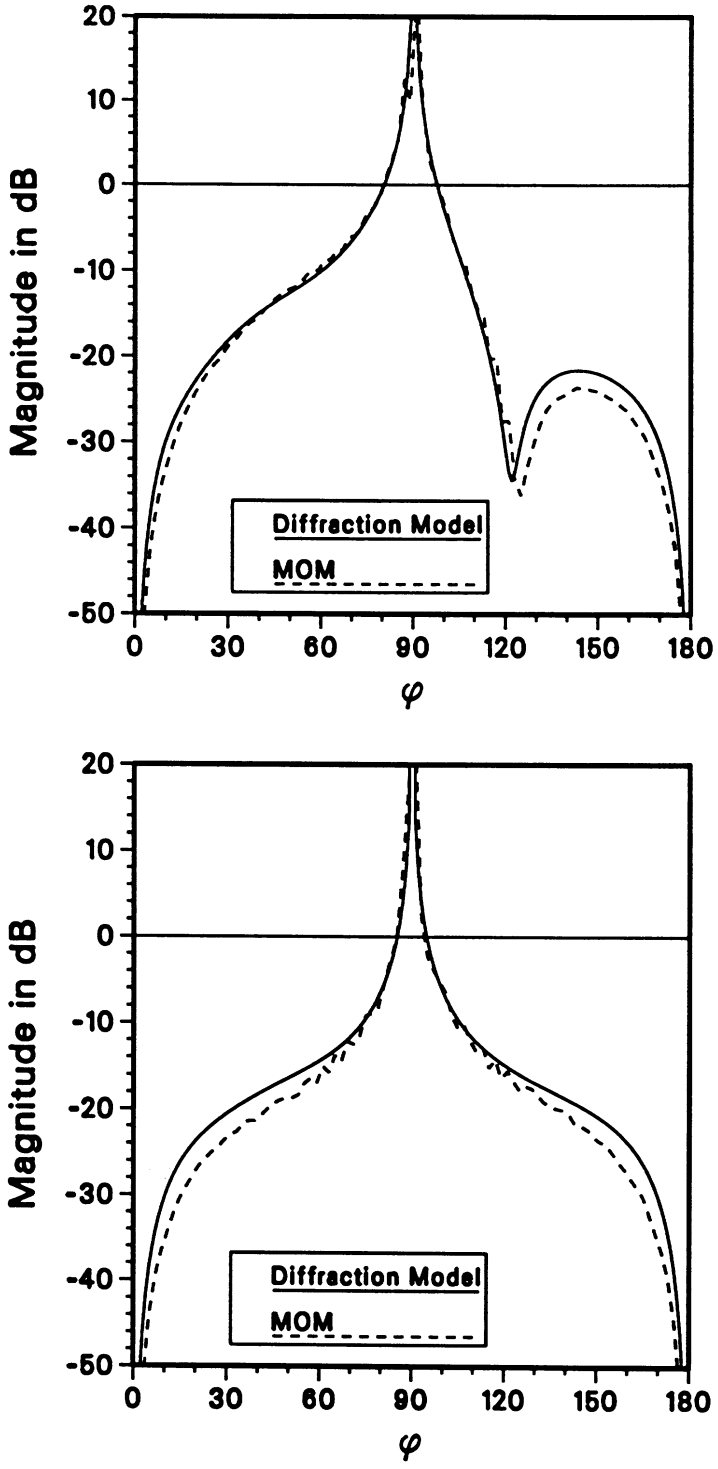

Figure 14: Comparison of backscatter as computed by the method of moments and higher order diffraction solutions of the original structure with $R = R_1 = Z_0/4$. (a) $d = 0.1\lambda$, $W = 0.5\lambda$ (top); (b) $d = 0.05\lambda$, $W = 0.1\lambda$ (bottom).

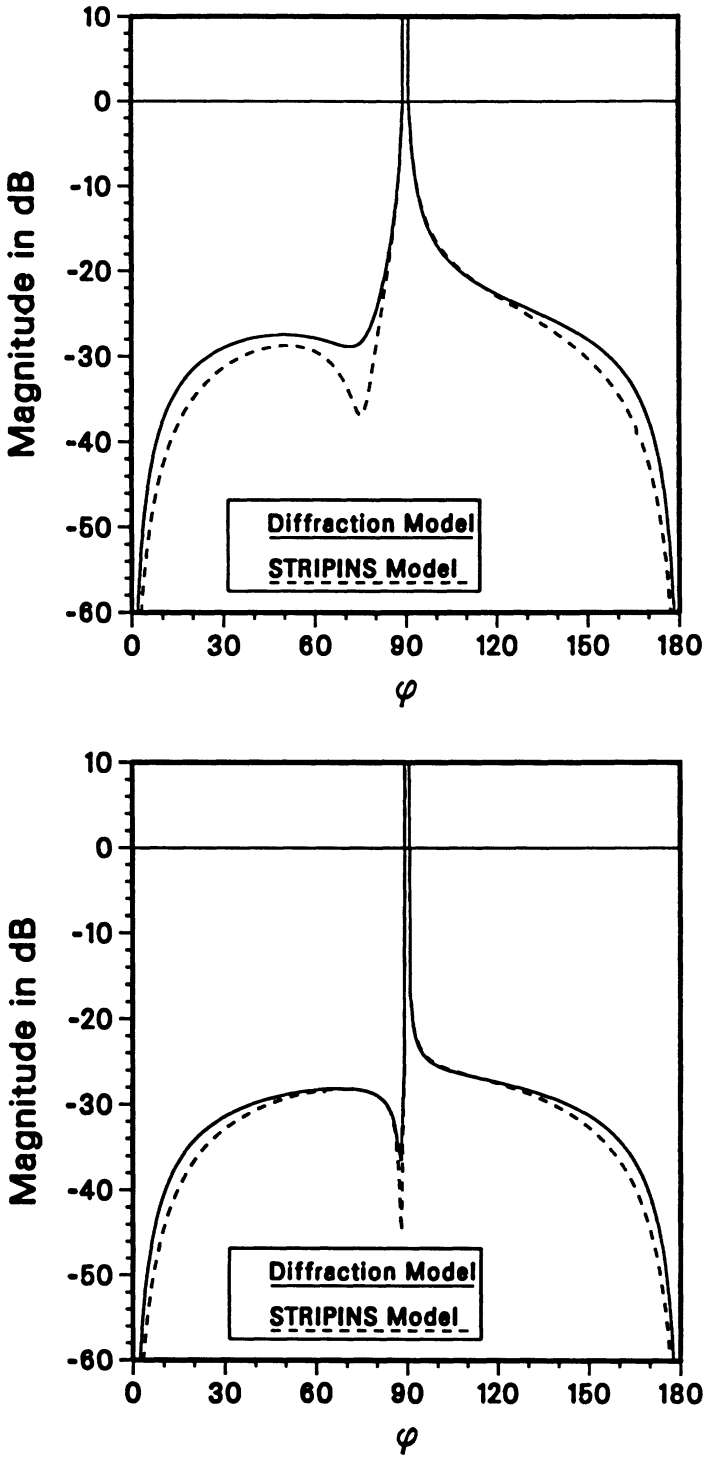

Figure 15: Comparison of backscatter RCS curves for the higher order diffraction and simplified model solutions with $R = R_1 = Z_0/4$. (a) $d = 0.01\lambda$, $W = 0.2\lambda$ (top); (b) $d = 0.001\lambda$, $W = 0.15\lambda$ (bottom).

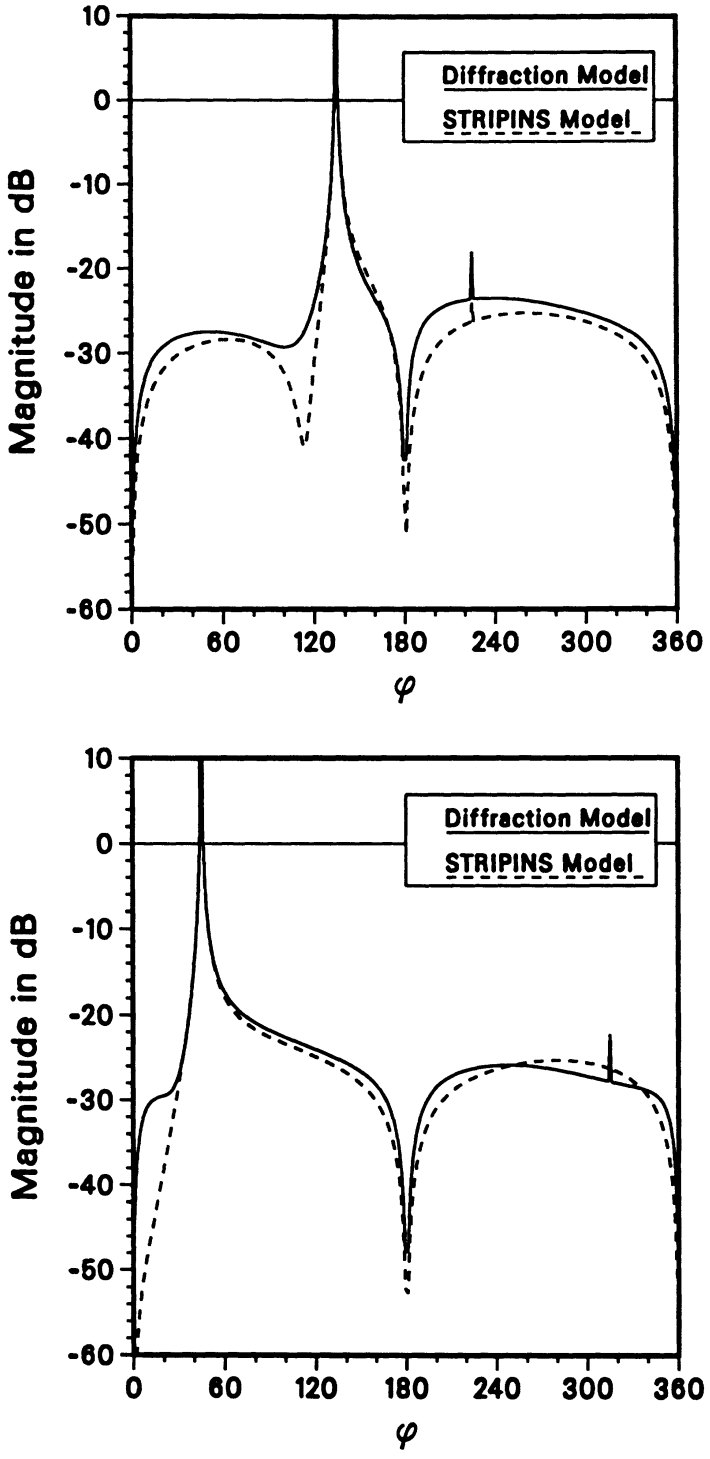

Figure 16: Comparison of bistatic patterns for the higher order diffraction and simplified model solutions with $R = R_1 = Z_0/4$, $d = 0.01\lambda$, and $W = 0.2\lambda$. (a) $\phi_0 = \pi/4$ (top); (b) $\phi_0 = 3\pi/4$ (bottom).

Acknowledgement

The authors are indebted to Leo C. Kempel for his assistance in generating a portion of the moment method data included in this report.

References

[1] H.G. Booker and P.C. Clemmow (1950), "The concept of an angular spectrum of plane waves and its relation to that of polar diagrams and aperture distribution," *Proc. Inst. Elect. Eng.,* **97**, pp. 11–17.

[2] P.C. Clemmow (1953), "Radio propagation over a flat earth across a boundary separating two different media," *Phil. Trans. R. Soc. London, Ser. A,* **246**, pp. 1–55.

[3] M.A. Ricoy and J.L. Volakis (1991), "Diffraction by a multilayer slab recessed in a ground plane via generalized impedance boundary conditions," *Radio Sci.,* **26** (2), pp. 313–327.

[4] M.A. Ricoy and J.L. Volakis (1992), "Diffraction by a symmetric material junction," *IEEE Trans. Antennas Propagat.,* July.

[5] Y. Sunahara and T. Sekiguchi (1981), "Ray theory of diffraction by a half-sheet parallel to a flat earth," *Radio Sci.,* **16** (1), pp. 141–155.

[6] J.L. Volakis and J.D. Collins (1990), "Electromagnetic scattering from a resistive half plane on a dielectric interface," *Wave Motion,* **12**, pp. 81–96.

[7] T.B.A. Senior (1985), "Combined resistive and conductive sheets," *IEEE Trans. Antennas Propagat.,* **AP–33**, pp. 577-579.

[8] J.L. Volakis and M.A. Ricoy (1989), "H-polarization diffraction by a thick metal dielectric join," *IEEE Trans. Antennas Propagat.,* **AP–37**, pp. 1453–1462.

[9] M.A. Ricoy and J.L. Volakis (1989), "E-polarization diffraction by a thick metal-dielectric join," *J. Electromagn. Waves Appl.,* **3**, pp. 383, 407.

[10] T.B.A. Senior (1975), "Half plane edge diffraction," *Radio Sci.,* **10** (16), pp. 645–650.

[11] P.C. Clemmow (1951), "A method for exact solution of a class of two dimensional diffraction problems," *Proc. Roy. Soc. A,* **205**, pp. 286–308.

[12] T.B.A. Senior (1952), "Diffraction by a semi-infinite metallic sheet," *Proc. Roy. Soc. (London),* **A 213** (1115), pp. 436–458.

[13] J.L. Volakis (1988), "High frequency scattering by a thin material half plane and strip," *Radio Sci.,* **23** (3), pp. 450–462.

[14] T.B.A. Senior (1990), "Diffraction by a material junction," Radiation Laboratory, Univ. of Michigan, Ann Arbor MI, RL–880.

[15] M.I. Herman and J.L. Volakis (1987), "High frequency scattering by a resistive strip and extensions to conductive and impedance strips," *Radio Sci.,* **22** (3), pp. 335–349.